Article

Thermal Sensor Calibration for Unmanned Aerial Systems Using an External Heated Shutter

Jacob Virtue [1,2,*], **Darren Turner** [1], **Guy Williams** [2], **Stephanie Zeliadt** [2,3], **Matthew McCabe** [4] and **Arko Lucieer** [1]

1 School of Geography, Planning, and Spatial Sciences, University of Tasmania, Hobart 7001, Australia; darren.turner@utas.edu.au (D.T.); arko.lucieer@utas.edu.au (A.L.)
2 AeroSpec, Sumner, Queensland 4074, Australia; guy@aerospec.com.au (G.W.); stephanie.zeliadt@csiro.au (S.Z.)
3 Commonwealth Scientific and Industrial Research Organisation, Hobart 7004, Australia
4 Climate and Livability Initiative, King Abdullah University of Science of Technology, Thuwal 23955, Saudi Arabia; matthew.mccabe@kaust.edu.sa
* Correspondence: jacob.virtue@utas.edu.au

Abstract: Uncooled thermal infrared sensors are increasingly being deployed on unmanned aerial systems (UAS) for agriculture, forestry, wildlife surveys, and surveillance. The acquisition of thermal data requires accurate and uniform testing of equipment to ensure precise temperature measurements. We modified an uncooled thermal infrared sensor, specifically designed for UAS remote sensing, with a proprietary external heated shutter as a calibration source. The performance of the modified thermal sensor and a standard thermal sensor (i.e., without a heated shutter) was compared under both field and temperature modulated laboratory conditions. During laboratory trials with a blackbody source at 35 °C over a 150 min testing period, the modified and unmodified thermal sensor produced temperature ranges of 34.3–35.6 °C and 33.5–36.4 °C, respectively. A laboratory experiment also included the simulation of flight conditions by introducing airflow over the thermal sensor at a rate of 4 m/s. With the blackbody source held at a constant temperature of 25 °C, the introduction of 2 min air flow resulted in a 'shock cooling' event in both the modified and unmodified sensors, oscillating between 19–30 °C and -15–65 °C, respectively. Following the initial 'shock cooling' event, the modified and unmodified thermal sensor oscillated between 22–27 °C and 5–45 °C, respectively. During field trials conducted over a pine plantation, the modified thermal sensor also outperformed the unmodified sensor in a side-by-side comparison. We found that the use of a mounted heated shutter improved thermal measurements, producing more consistent accurate temperature data for thermal mapping projects.

Keywords: thermal mapping; infrared; temperature measurements; FLIR Vue Pro R; thermal capture calibrator; UAV; UAS; drone; RPAS

1. Introduction

1.1. Thermal Sensors and UAS

UAS-mounted sensors are increasingly being used for a range of environmental, agronomic and forestry applications [1–3] and have also enhanced our capacity to monitor wildlife. Compared to manned aerial and satellite-based remote sensing, UAS-mounted sensors can acquire real-time, high-resolution imagery at relatively low cost. Apart from the resolution advantage over satellite systems, UAS-mounted thermal infrared sensors can deliver non-destructive, non-contact thermal maps of study areas in ways that were not previously possible.

Thermal sensors have great potential for use in a variety of applications requiring accurate temperature data at high spatial and temporal resolution [4–8]. Applications include detection of disease infestations in forest canopy [3], assessing water stress in

crops [7], and investigating transpiration and temperature fluxes of land surfaces [9]. Wildlife studies are increasingly utilising thermal UAS technology such as census surveys of hippopotami in the Congo [10], grey seals in Canada [11], and roosting fruit bats in Australia [12], reducing time and effort associated with population studies.

Constraints on UAS payload capacity and sensor power consumption are major considerations in sensor utility. The use of microbolometer sensors without temperature stabilisation enables thermal sensors to be small, lightweight, and energy efficient compared to cooled thermal sensors [13,14]. Commercially available UAS-mounted thermal infrared sensors can achieve accuracies of ± 5 °C or 5% of the sensor reading [15], depending on the target. However, this is often inadequate for applications such as crop water stress measurements that may require accuracies of ± 1 °C [14]. These low-cost, uncooled thermal sensors are notoriously sensitive to temperature fluctuations across the sensor detector, sensor housing, and lens under ambient flight conditions. Depending on a range of factors, the housing of the sensor can heat up, resulting in a temperature increase in the detectors and electronics, which influence retrieval accuracy. Sensor temperature instability during flight results in thermal drift affecting acquired images. Correction for thermal drift must be applied continuously, otherwise the temperature error has been shown to increase by approximately 0.7–1.0 °C per minute [16].

The drift in thermal sensors and resulting fluctuations in the thermal response can go unnoticed within individual images. However, the merging of multiple overlapping thermal images in a structure-from-motion workflow can result in major errors in the production of thermal orthomosaics [17]. These errors will result in interpretation issues for both relative (qualitative) and absolute (quantitative) temperature measurements. This is particularly relevant when the temperature range in the scene only exhibits subtle variations, which can lead to inconsistent temperature measurements [13,18]. Consideration of other influencing factors, such as atmospheric absorption, reflectivity, emissivity, as well as the temperature changes within the thermal sensor, can all combine to affect the accuracy of temperature data acquired by thermal sensors [19].

1.2. Previous Studies Addressing Thermal Sensor Drift

Several post-processing approaches have been proposed to compensate for the thermal drift issues in UAS-mounted thermal infrared sensors. Budzier et al. [13] outlined mathematical and physical principles for the calibration of sensors, including non-uniformity correction, temperature dependence correction, defective pixel correction, shutter correction, and radiometric calibration. Ribeiro-Gomez et al. [20] developed calibration algorithms accounting for the temperature of the sensor and the digital response of the microbolometer that reduced the error from 3.6 °C to 1.4 °C [20]. To increase measurement accuracy and reduce vignetting effects, Aragon et al. [17] developed an ambient temperature-dependent radiometric calibration function in the laboratory using a modulated blackbody source with four discrete temperature steps. Mesas et al. [14] developed mathematical drift correction models that produced an error lower than 1 °C. As an in situ correction strategy, the captured images of ground reference sources of a known temperature before, during, and after flight, can also be used to post-process thermal images to correct for sensor temperature fluctuations [21–23].

Other approaches used to compensate for thermal drift are based on an internal shutter [18,21]. To correct for non-uniformities resulting in temperature inconsistencies, an image is taken with the shutter closed after a predetermined time interval or a temperature change in the shutter itself [14]. The main disadvantage of shutter-based compensation is the periodic loss of data when the shutter is closed. Olbrycht et al. [16] proposed replacing the opaque shutter, which blocks infrared radiation, with a semi-transparent one so as not to interrupt data acquisition during shutter closure. A common way to compensate for periodic data loss due to shutter closure is to increase the degree of forward overlap between images. However, this can increase flight time, which can result in a reduction in the area captured in the time available. Unlike visual image collection, thermal data

acquisition is far more prone to within-scene thermal variations as the collection time increases.

More importantly, non-uniformity shutter-based correction does not take into account temperature fluctuations in the sensor optics and lens, which are subject to influences from wind, shading, and other factors during flight [24]. Due to the drift issue inherent in thermal sensors, a system is needed to regularly and consistently re-calibrate the sensor as images are captured. Furthermore, the system needs to be able to compensate for both the ambient environmental temperature fluctuations and those from the thermal sensor itself.

1.3. This Study

Precise in situ temperature data captured during a flight negates the need for downstream thermal image correction, thereby reducing post-processing time. One possible means of achieving this is the use of a heated shutter that can be externally installed on UAS-mounted thermal sensor to facilitate a uniform calibration target. Externally heated shutters used for thermal imaging, such as the Thermal Capture Calibrator (TCC)(TeAx Technology, 'ThermalCapture Calibrator', TeAx Technology GmbH, Wilnsdorf Germany, https://thermalcapture.com/thermalcapture-calibrator/, (accessed 27 June 2021), are reported by the manufacturer to increase the temperature accuracy for absolute temperature measurement by up to 70% in radiometric thermal maps [25]. To date, there has been limited research on the use of these shutters, hence rigorous laboratory and field testing is needed to assess their performance

The aim of this study was to evaluate and compare the stability and accuracy of thermal imaging sensors with and without an external heated shutter. A high-quality temperature modulated blackbody source was utilised in a laboratory setting in order to compare a thermal sensor modified with a heated shutter to an unmodified thermal sensor. Controlled temperature experiments were performed over time, along with tests that reproduce operational wind conditions. In addition, a separate field-based evaluation was undertaken with both the modified and unmodified thermal sensors being flown simultaneously over a pine tree plantation. We did not assess absolute temperature performance in the field trials. For the field application, the focus was on examining the temperature variability of the modified thermal sensor relative to the unmodified sensor rather than assessment of absolute temperature accuracy. Finally, a set of guidelines for the use of UAS-mounted thermal sensors modified with a heated shutter is provided, along with a framework for initialisation and field deployment.

2. Data and Methodology

2.1. Laboratory Tests and Equipment

2.1.1. Thermal Sensor and Thermal Capture Calibrator

The FLIR Vue Pro Radiometric (FVPR-FLIR Systems, Inc., Wilsonville, USA) uncooled micro-bolometer thermal imaging sensor was used in this study (Figure 1). The FVPR, which is specifically designed for UAS-based remote sensing, has a 640×512 pixel sensor with a 13 mm lens, and was programmed to capture TIFF images every 2 s of the survey. The sensor images across the 7.5–13.5 μm spectral range, and has a manufacturer specified accuracy of ± 5 °C or 5% of the sensor reading. This sensor conducts unconfigurable non-uniformity corrections at approximately 30 s intervals, or as determined by the camera. In flight, this sensor was powered by the UAS auxiliary power supply. The external heated shutter used in this study was the Thermal Capture Calibrator (TCC) (Figure 1). The TCC was mechanically integrated onto the FVPR and has a heated external shutter that closes over the thermal sensor lens every 20 s to conduct a flat field correction (FFC) that provides an accurate and uniform calibration. The advertised feature of the TCC is that it increases the accuracy of absolute temperature measurement by up to 70%. The radiometric settings of each sensor were set to the same operating parameters of Target range: 45 m, Humidity: Medium, Air Temp: 20 °C, Sky Condition: Clear.

Modified   Unmodified

Figure 1. The Flir Vue Pro R with ThermalCapture camera calibrator mechanically attached to sensor (modified) and the Flir Vue Pro R (unmodified) (Source TeAX, Flir).

2.1.2. Laboratory Configuration

The laboratory-based measurements were performed in an air-conditioned room to maintain a constant humidity and temperature of 20 °C for all experiments that was stabilised for 1 h prior to data collection. The laboratory was painted matte black with all external light sources blocked out. The temperature was monitored using an auxiliary logger to confirm that the ambient diurnal temperature variation was within ±0.5 °C (LogTag Temperature Logger HAX0-8). In addition to the ambient temperature, a contact temperature probe was used to monitor the temperature of the exterior housing of the sensor (Center 376 Data Logger).

A high emissivity cavity blackbody source (Isotech Hyperion R Model 982) was used to test and calibrate the FVPR and FVPR+TCC. The physical parameters of the blackbody include a 50 mm aperture and 150 mm cavity. The primary radiation source has an adjustable temperature range of -10 °C to 80 °C. The blackbody temperature was logged via the built-in temperature indicator and an external platinum resistance thermometer. The blackbody source was turned on 30 min prior to data capture to allow source temperature stabilisation. The blackbody source maintained the set temperature to within ±0.1 °C. Test parameters of the blackbody (temperature and time) were automatically controlled using *Caliso Temps* software (Humage Technology LTD). Each experiment utilising the blackbody source was repeated with both sensors (FVPR and the FVPR + TCC).

Blackbody temperature variation tests were conducted for the laboratory-based calibration experiments. Sensor configurations (i.e., FVPR with and without the TCC) were compared at a constant blackbody temperature of 35 °C for 4 h to first assess sensor performance under stable conditions. The FVPR that had been modified with the TCC thermal calibrator (FVPR+TCC) and the unmodified FVPR were installed 5 cm away from the aperture of the blackbody to ensure that the entire sensor frame was exposed to the blackbody source. Both sensors were tested individually with image capture at a frequency of 0.5 Hz. The equation used for temperature value conversions of the thermal image from digital number (DN) to °C is [15]:

$$T\ brightness = DN * 0.04 - 273.15 \tag{1}$$

2.1.3. Simulating Operational Wind Conditions

To simulate the horizontal wind-gradient expected in the field, (i.e., whilst the UAS was moving over the survey area) the thermal sensor was exposed to simulated wind in the laboratory. The wind produced by a brushless electric motor with a small propeller. The speed of the brushless motor was adjusted to achieve a consistent wind flow of 4 m/s over the housing of each thermal sensor and measured with an anemometer to within an accuracy of ±0.2 m/s (Protec QM1646). The 4 m/s wind flow was introduced for a period of 2 min, then removed for 2 min, to simulate upwind (into headwind) and downwind (with a tail wind) flight lines.

2.2. Field Tests

2.2.1. UAS and Flight Planning

A DJI Matrice M600 (DJI, Shenzhen, China) was used as the UAS platform. The M600 can accommodate two thermal sensors (FVPR and FVPR+TCC) data collection. Mission planning and flight path calculation was programmed with DJI Ground Station Pro version 2.0.15 (GS Pro). This application controlled the path and speed for the duration of the mission and ensured the calculated survey parameters were followed. The UAS maintained a specified heading for the duration of the survey, which was user-selected to optimise flight performance. The UAS maintained a constant flying height above take-off elevation of 45 m. The terrain variation within the study area was ± 7 m. The overlap used for the missions was 80% along-track and 80% across-track for the field of view of the FVPR, which resulted in a flight speed of 4 m/s and flight lines 10 m apart. The speed of 4 m/s was utilised to ensure that forward speed of the UAS did not cause motion blur in the thermal imagery.

2.2.2. Field Operations

Four flights were conducted over a two-year old pine plantation (*Pinus radiata*, 1.5–2 m tall trees) in the Upper Castra region in central Tasmania, Australia, between November 19–20, 2019. Flights were conducted at noon and 2 pm at 40 m above ground level, with an approximate duration of 15 min each. The 9 am and 3 pm air temperature on November 19 was 12.8 and 19.6 °C, respectively, with a corresponding wind speed of 3.06 and 1.94 m/s. The 9 am and 3 pm air temperatures on November 20 were 12.5 and 15.4 °C, with wind speed of 3.61 and 1.67 m/s, respectively (see data for Station 091291, approximately 17 km from the study site at http://www.bom.gov.au/climate/dwo/index.shtml (accessed on 21 March 2021)). Both sensors were mounted on the same UAS and flown together, capturing data simultaneously. Digital numbers from the thermal data collected in the field were converted to temperature using the listed equation (2.2.1).

2.3. Image Processing

2.3.1. Blackbody Imaging

Images captured during the blackbody experiments were at a rate of 0.5 Hz for a duration up to 2.4 h. The central kernel of each image was defined as the centre 9×9 pixels and was used to avoid any distortions or aberrations resulting from the sensor lens, e.g., vignetting, variability in the sensor to blackbody alignment, or non-uniformities of the blackbody source. The mean digital number of this kernel was converted to temperature using the listed equation (2.2.1).

2.3.2. Vignetting Filter

To address the known vignetting error associated with this sensor, a filter was created. This filter captured stable blackbody temperatures over a period of 1 h. This image set was averaged pixel-wise and divided by the total average of all pixels in the center 30% of the image to produce a scale factor for each pixel. The vignetting filter was created for both sensors with the average pixel value within 0.7% for the unmodified sensor and within 0.1% for the modified sensor. This filter was applied to the images captured by the unmodified sensor.

2.3.3. Orthomosaics and Orthophotos

M600 flight information, including GNSS data, were logged during each mission and stored onboard. These files were downloaded and converted using DatCon (version 3.6.3) into .csv files at a sample rate of 0.5 Hz to match the frequency of the images captured by the FVPR. Images were geotagged with the GNSS latitude, longitude, altitude, and time for the duration of the flight synchronized with the time that the FPVR images were captured.

Orthomosaics were created from the thermal images using AgiSoft PhotoScan (Version 1.4.4). Images were aligned using the following default settings: highest accuracy, generic

preselection, key point limit = 40,000 and tie point limit = 4000. Aligned images were used to create a mesh with the following settings: surface type: height field (2.5 D), face count: 'high' (90,000) and interpolation enabled. These settings were used to achieve a pixel size of 3 cm. The final orthomosaics were then analysed in QGIS software (version 3.6.2).

The orthomosaics were comprised of a series of individual orthophotos. Due to the high overlap used for the flights, each pixel within an orthomosaic was imaged 4–40 times, depending on the location in which the image was captured. Pixels in the centre of the orthomosaic were imaged more frequently than pixels on the outer edges. The individual orthophotos (i.e., an orthorectified version of each individual image frame) were exported from Agisoft Photoscan for analysis. After export, there were 650–730 orthophotos for each flight (dependent on the size of the survey area).

### 2.3.4. Orthophoto Image Calculations

To quantify thermal variability, the temperature observed at each unique coordinate within the orthomosaic was calculated. As each pixel was observed from multiple angles and positions, an unbiased mean standard error was returned at each unique location. The orthophotos were imported into Python (version 3.6) with rasterio (version 1.0.21), and the digital number of each pixel was stored in multi-dimensional arrays and indexed with easting and northing values. Digital numbers (DN) with values of 0 or 65,353 were removed, as they were erroneous 'no data' points resulting from the photo alignment and orthophoto export. The size of the resultant array was 180–250 million points, depending on survey area. Using standard python libraries (numpy (version 1.16.4), rasterio (version 1.0.21), xarray (version 0.15.1), pandas (version 0.24.2), bokeh (version 2.1.1), dask (version 2.1.0), datashader (version 0.11.1), and holoviews (version 1.13.4), multi-dimensional array calculations were achievable without the use of a high-performance computing system. Datashader was used to visualise results by aggregating all the values for each unique easting and northing location from all the overlapping images. Calculations used to aggregate values included count, standard mean error, minimum, maximum, and mean values.

3. Results

The study comprised both laboratory and field-based experiments. Laboratory experiments were conducted to quantify the difference between the performance of a modified thermal sensor (i.e., with a mounted heated shutter) and an unmodified sensor, both of which were housed in a controlled environment. Field-based mapping missions were conducted under typical environmental conditions expected during normal operations (i.e., wind and ambient temperature fluctuations).

3.1. Laboratory-Based Experiment

During the laboratory trial, the blackbody was warmed up for 30 min in order to reach and maintain a stable temperature reading of 35 °C. Both sensors had a warm-up stabilisation period of 20 min. Analysis of the centre pixel values of the thermal imagery (Figure 2) demonstrates that the modified and unmodified sensors measured the blackbody with temperature ranges of 34.3–35.6 °C and 33.5–36.4 °C, respectively, over the 2.4 h testing period. Standard deviations throughout the testing period of the modified and unmodified sensors were ±0.19 and ±0.46, respectively. The logged room temperature was ±0.24 °C and contact temperature for the thermal sensor was ±0.37 °C throughout the duration of the experiment.
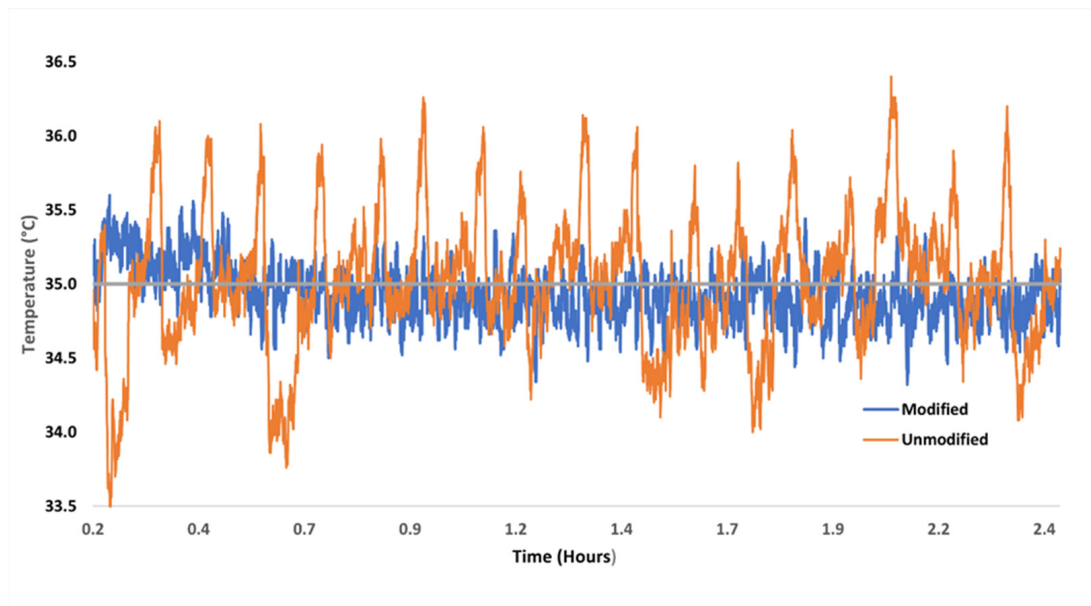
Figure 2. Laboratory-based temperature trial, where the blackbody was held at 35 °C (grey line). FLIR Vue Pro R with the ThermalCapture camera calibrator (Modified) and the FLIR Vue Pro R without the ThermalCapture camera calibrator (Unmodified) temperature ranges are plotted for the duration of the experiment.

During the air flow trial, the blackbody source was held at a constant 25 °C to simulate local ambient summer operating temperatures for the duration of the experiment. A wind field of 4 m/s was introduced for periods of 2 min to simulate 480 m flight lines typical of in-flight field conditions. The results of the test comprised four phases: (1) the initial sensor stabilisation phase, (2) the first introduction of wind flow producing a 'shock cooling' event, (3) the subsequent introduction of airflow simulating inflight conditions, and (4) the sensor stabilisation phase after wind flow ceased (Figure 3).
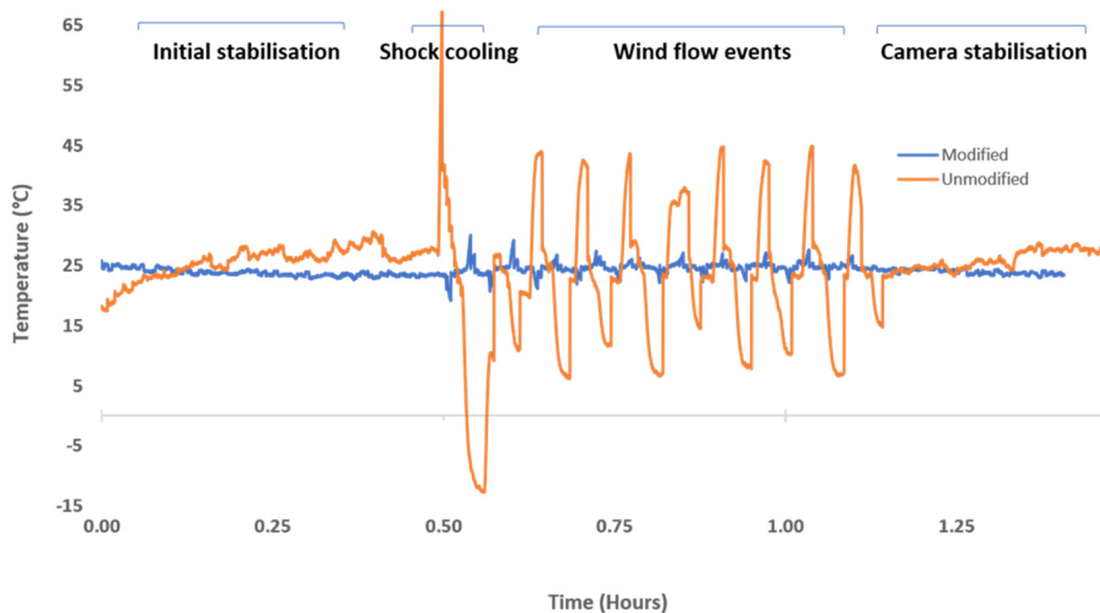
Figure 3. Air flow trial using the FLIR Vue Pro R with the ThermalCapture camera calibrator (modified) and the FLIR Vue Pro R without the ThermalCapture camera calibrator (unmodified). The blackbody was held at 25 °C with an introduced air flow (4 m/s).

In the initial sensor stabilisation period (30 min), temperatures measured by the modified and unmodified sensors were maintained at 25 ±2 °C and 25 ±10 °C, respectively. For the 'shock cooling' event, the unmodified sensor showed a severe deterioration in temperature recordings, oscillating markedly between -15 and 65 °C, and then oscillated between 5 and 45 °C for the subsequent airflow events. The temperature of the modified sensor during the 'shock cooling' event oscillated between 19 and 30 °C, and then maintained a temperature between 22 and 27 °C for the subsequent airflow events (Figure 3).

3.2. Field Based Experimentation

Orthomosaics of a representative flight using the modified and unmodified sensors flown in tandem on a single platform are depicted in Figure 4a,b. The vignetting filter of Section 2.3.2 was applied to data captured via the unmodified sensor. Digital numbers for each pixel at each unique easting and northing coordinate were converted to temperature using the formula provided in Section 2.2.1. Each pixel value is composed of 4 to 40 observations from different angles, and the variation in temperature for each pixel was measured by its standard mean error for each unique coordinate (Figure 4a,b). The pine trees can be seen in the thermal orthomosaic as dark circles. An orthomosaic showing the flight path of the study site is depicted in Figure 4c, showing the nine transect lines flown, with the start and finish points indicated.

The histogram in Figure 4a,b shows the amount of temperature variation in the data set. The histograms contain 20 bins of standard mean errors derived from the temperature values of the thermal data from the modified and unmodified thermal sensors. The modified thermal sensor was better able to maintain consistent temperatures throughout the flights, whereas the temperature of the unmodified sensor fluctuated with changes in ambient temperature during the flight.

Temperature variations (as measured by standard mean error) are variable across the plantation. However, the unmodified sensor was more variable, as can be seen by the coloured striations in the orthomosaic (Figure 4a). The dark red area in the lower left clearly shows the 'shock cooling' event at the start of the mapping operation (Figure 4a). The 'shock cooling' event was not as apparent in the data from the modified sensor (Figure 4b). The larger standard mean error from the modified sensor was primarily due to pine tree edge effects (dark rings) that was also evident in the data from the unmodified sensor. This was a result of minor misalignments and angular observations between the different orthophotos, highlighting the edges of the tree canopies.

Results obtained from all four flights in Figure 5 show the standard mean errors of the modified sensor to be consistently smaller compared to the unmodified sensor on the same flight. The median standard mean error from the modified and unmodified sensor ranged from 0.23–0.63 °C and 0.58–1.25 °C, respectively. The flight with the smallest range of error had an interquartile range of 0.23 °C (flight 2) using the modified sensor, compared to the unmodified sensor 0.77 °C for the same flight. The flight with the largest range in error had an interquartile range of 0.63 °C using the modified sensor, and 1.25 °C using the unmodified sensor (flight 4).
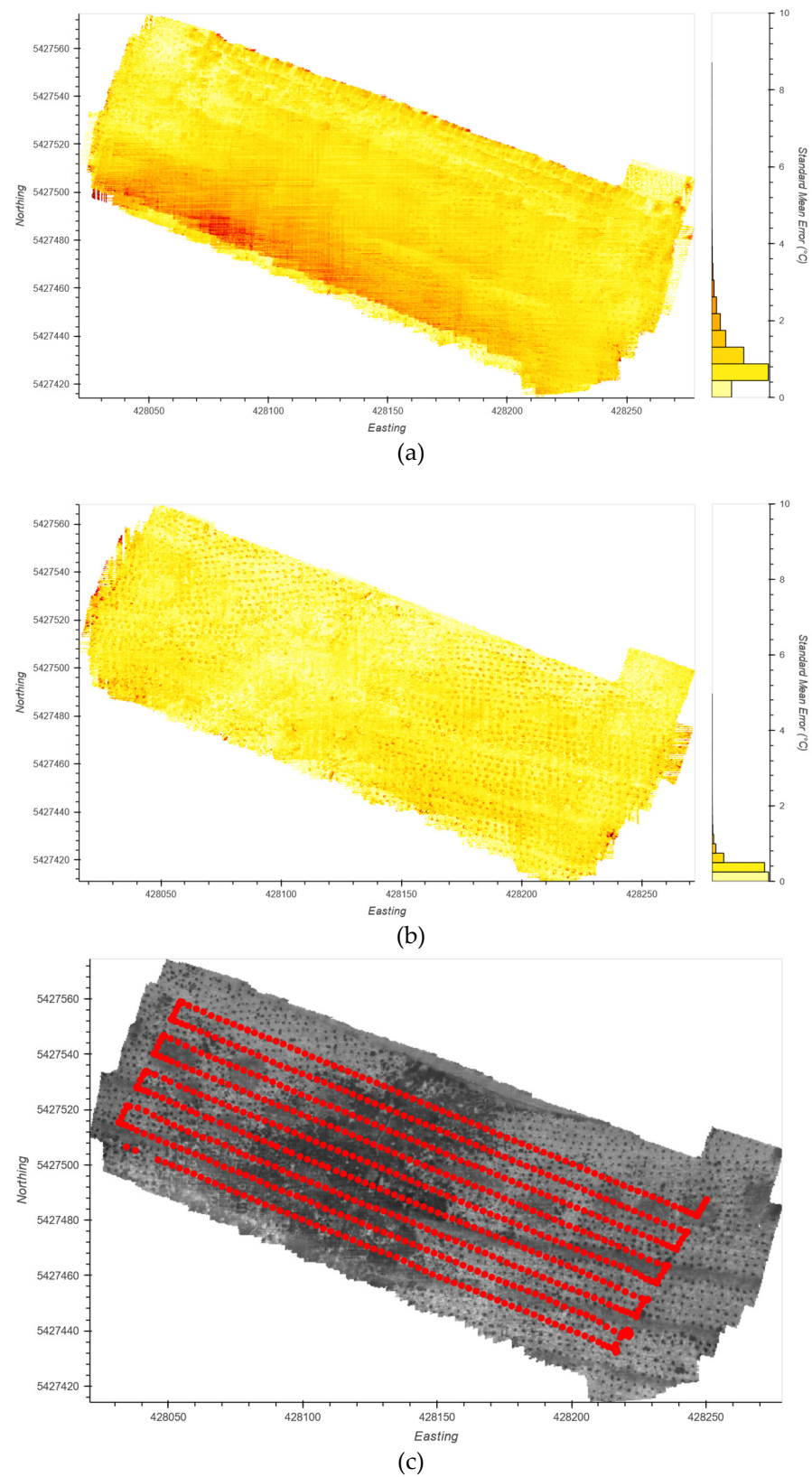
Figure 4. Thermal orthomosaics of a flight over a pine plantation and histogram showing temperature (°C) standard mean error at each unique pixel locations and variation that occurs during mapping conditions for (**a**) FLIR Vue Pro R without the ThermalCapture camera calibrator (unmodified) (**b**) FLIR Vue Pro R with the ThermalCapture camera calibrator (modified). The flight path (**c**) over the study site shows transect lines and start and end points overlaying a thermal image of the study area.
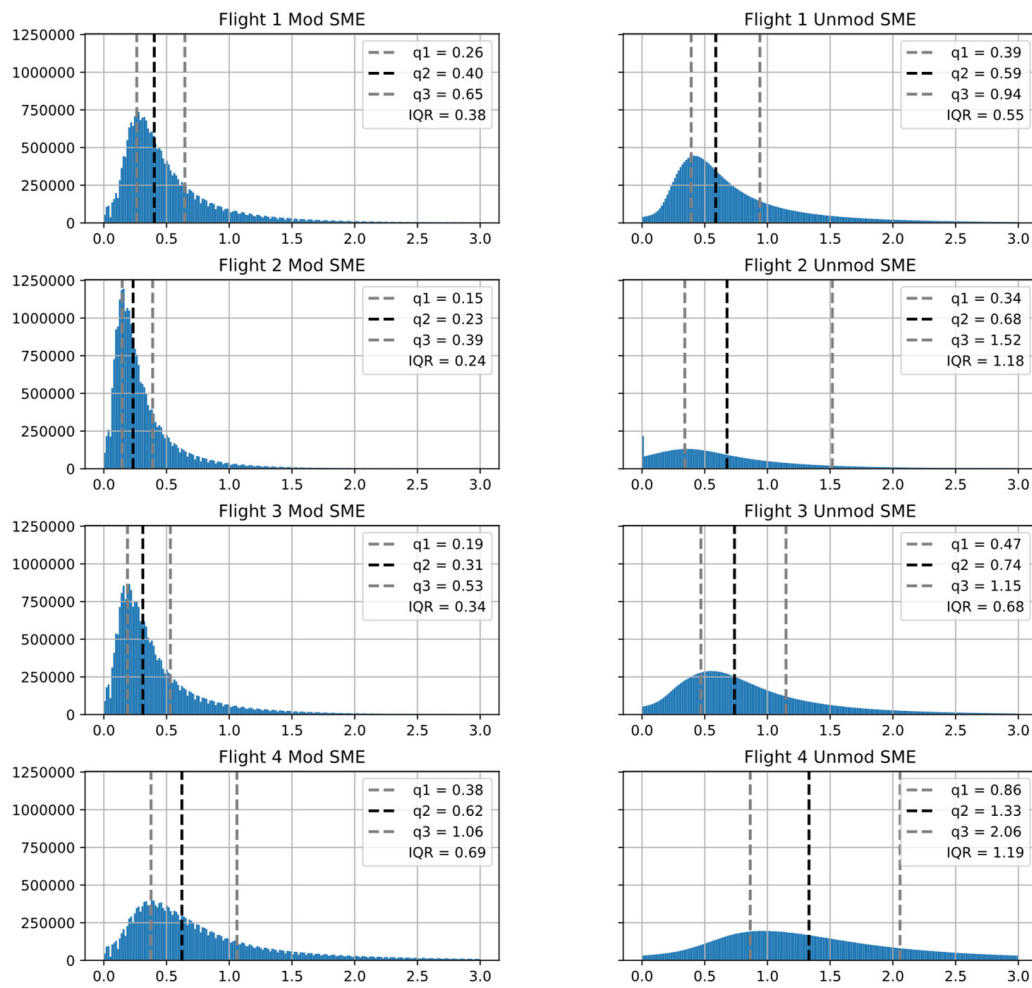
Figure 5. Standard mean error (°C) for four flights over a pine plantation using FLIR Vue Pro R with the ThermalCapture camera calibrator (modified) and the FLIR Vue Pro R without the ThermalCapture camera calibrator (unmodified). Quartile 1—grey dashed line, quartile 2—black dashed line, and quartile 3—grey dashed line.

4. Discussion

Several approaches have been used to correct for sensor temperature fluctuations in uncooled thermal sensors, the majority of which require some degree of post-processing [18,21–23]. To compensate for sensor detector drift during flight, shutter [13] and shutter-less [18] non-uniformity corrections have been used, both of which require considerable calibration effort. In this study, we used a heated external shutter (TCC) that resets a sensor's thermal range. This TCC self-calibration procedure occurs by performing a flat field correction every 20 s via the closing of a heated shutter, which is far more frequent than the non-uniformity correction performed by the thermal sensor alone. Our experimental results, measuring a reference blackbody temperature, showed a marked increase in the accuracy of the thermal data acquired using the modified sensor compared to the unmodified sensor, alleviating the need to conduct corrections during post-processing.

4.1. Laboratory Calibration

The performance of the thermal sensor in this study, with the heated shutter against a temperature modulated blackbody source, consistently provided more uniform thermal imaging performance. At a constant blackbody temperature, the modified thermal sensor maintained stable temperature recordings (±0.5 °C) over the duration of the experiment, compared to the unmodified thermal sensor, which showed fluctuations in the temperature recordings as high as ±4.0 °C.

Limited comparative studies have been conducted testing the performance of thermal sensors, and it is difficult to directly compare our results with others due to differences in experimental design. A recent paper by Aragon et al. [17] compared infrared sensors against a modulated blackbody target to determine temperature dependent radiometric calibration equations used to increase the accuracy of thermal data. Application of these calibration functions resulted in a marked improvement in the accuracy of thermal temperature data. They compared the FLIR A655sc, TeAx 640, and Apogee sensors by applying derived calibration matrices to correct each pixel, which improved the accuracy from a root mean squared error of 6.2 to 0.8 °C and 3.4 to 1.0 °C, respectively, over a temperature range between 0–60 °C.

Current automatic non-uniformity corrections performed by thermal sensors do not remove vignetting effects [17,26]. Aragon et al. [17] suggested that to obtain accuracies within 1 °C, thermal imagery needs to be calibrated after data collection. Such calibration involves a substantial laboratory setup to produce multiple temperature references to derive multilinear regression equations. These calibration equations were derived by using an array of resistance detectors at various temperatures to measure temperatures of a blackbody. As we show in the present study, the use of a heated shutter on a thermal sensor shows promising initial results, which may eliminate the need to undertake extensive calibration procedures as it undertakes a self-calibrating regime in situ.

Under the simulated wind flow conditions in this study, both the modified and unmodified thermal sensors experienced 'shock cooling' events with initial temperature recordings fluctuating between ±10 °C and ±40°C, respectively. Kelly et al. [26] used a FLIR Vue Pro 640 and subjected it to sustained wind treatments under laboratory conditions. They reported that the sensor experienced a temperature recording change of > 20 °C and did not stabilise for 15 min. In our study, the modified thermal sensor was more tolerant than the unmodified sensor when subjected to subsequent 'shock cooling' resulting from the introduction of wind. However, it still required a post-event stabilisation period of approximately 3 min for accurate temperature measurements. The modified sensor consistently outperformed the unmodified sensor with smaller temperature errors.

These larger temperature errors with the unmodified sensor seen in this study are a result of inadequate non-uniformity correction of the microbolometer focal plane array [16,27]. The effect of wind causes a change in the shutter temperature, which is not always the same as the internal sensor temperature during flight. Non-uniformity correction does not account for this difference in temperatures. For this reason, as Kelly et al. [26] pointed out, non-uniformity correction may not be valid for UAS thermal imagery. The use of a heated shutter maintains a constant temperature, which alleviates this issue of temperature differences between the internal sensor and the shutter resulting from the influence of wind and external temperatures.

4.2. Field Operation

The modified thermal sensor with the heated shutter outperformed the unmodified thermal sensor when flown simultaneously on a single UAS platform in field trials. The temperature variability for pixels in the thermal orthomosaic, as revealed by the standard mean errors, were substantially smaller with the modified thermal sensor compared to the unmodified thermal sensor. The thermal orthomosaics from the unmodified sensor showed substantial striations in output due to the sensor changing temperature during the mapping mission. The unmodified thermal sensor was unable to maintain consistent temperatures throughout the flights due to the temperature of the sensor fluctuating with ambient flight conditions. This result was consistent with the laboratory simulated wind flow trials, particularly during the initial 'shock cooling' event and subsequent wind flow treatments.

Results from the present study suggest that, although extensive stabilisation is not required in the field, a short (2–3 min) flight at mapping speed of 4 m/s, should be conducted prior to initiating the thermal mapping mission. This exercise allows the sensor

to initially warm up, and then be 'shock cooled' to the ambient operating temperature to achieve thermally accurate images. This short pre-calibration period, where the sensor reaches thermal equilibrium, can be equivalent to the time required for the UAS to lift off and transit to the first transect and hence there could be minimal loss of survey time.

Lengthy stabilisation periods whilst the UAS is airborne will significantly reduce flight time and limit the area covered by an individual flight. Smigaj et al. [3] recommended a 30–60 min stabilisation period and Kelly et al. [26] recommended a 15 min (preferably one hour) stabilisation period due to the large shift in the digital number after sensor activation. Stabilisation periods of this length of time are impracticable for field-based data collection. Using the heated shutter, there was no such dramatic shift in sensor digital number, reducing the need for lengthy stabilisation periods.

Other approaches used to compensate for thermal drift include the use of calibration models derived from ground reference stations along the flight path [1,26]. These studies suggested flying over ground calibration targets of known temperatures throughout the mission, which are subsequently used for post-flight processing to correct for temperature drift. Using ground reference stations, both Pestana et al. [23] and Gomez-Candon et al. [1] achieved a 1 °C accuracy. Similarly, Acorsi et al. [27] derived individual models from datasets from missions flown at specific heights and times of day resulting in improved accuracy with values ranging from 1.32 to 1.94 °C. While deploying ground reference stations to correct for temperature bias may not be necessary when using a thermal sensor with a mounted heated shutter, further field studies need to be conducted to verify this.

The use of the modified sensor during the field flights in the study resulted in more accurate temperature data compared to the unmodified sensor, as indicated by the interquartile range comparison of concurrent flights. This low level of variability is necessary for many applications such as precision agriculture or phenotyping, where water management is a major concern [14]. To detect drought tolerant trees, Ludovisi, et al. [28] used UAS-based thermal imaging applying field phenomics. Agricultural irrigation is the primary source of freshwater use in the world [7]. Crop water stress indices use the difference between air and canopy temperatures and require a high absolute accuracy in temperature observations [29–31]. Using low-cost, high-resolution thermal information would help better manage water resources.

In situations where near real-time irrigation management is required, efficient turnaround times from data acquisition to processing is advantageous for planning watering regimes. Our study shows that UAS-derived precision temperature data was acquired without any post-flight calibration delays. Using a thermal sensor without a heated shutter would inevitably result in delays for post-processing of data to compensate for temperature fluctuations of the sensor, body, and lens under ambient flight conditions. Although using radiometric calibrations for infrared thermal sensors can improve temperature accuracy [17] it requires a commitment to post-processing. Acquiring real time UAS-derived precision temperature data that can detect subtle temperature variation would be a valuable tool to assess crop water status, which has the potential to benefit many agricultural, forestry, and ecosystem monitoring applications.

The field trials conducted in this study were limited to four flights over a two-day period. Although the variability in flight 4 compared to 1–3 was noted, the variability between the modified and unmodified sensor within flight 4 was comparable to the results for flight 1–3. No environmental field parameters, such as wind and temperature, were considered in this preliminary investigation. As such, systematic field-testing under a range of different temperatures, wind directions and speeds, and flight patterns should be considered in future studies.

Further testing should also be undertaken over a uniform target such as a homogeneous agricultural field to reduce the confounding effects of topography and vegetation on ambient temperatures and reduce interference from anomalies, such as the edge effects from the pines as seen in this study. It will also be necessary to conduct new tests to validate the absolute temperatures measured by the sensor modified with a heated shutter. Future

work may include the automatic selection of shutter temperature based on prevailing environmental conditions. In addition, inter-sensor variability could be considered prior to conducting camera modifications.

4.3. Operational Recommendations

Based on the experimental findings of this study and operational experience, recommendations for optimal performance using a UAS mounted uncooled thermal infrared sensor modified with an external heated shutter include:

- Upon commencement of a mapping mission, fly for 2–3 min at a speed of 4 m/s prior to data collection to allow the sensor to be 'shock cooled' to ambient conditions;
- Although absolute temperature accuracy was not assessed in this study, deployment of thermal calibration targets is recommended at the beginning of the study to initially verify ground temperate. The temperature stabilising benefits of the heated shutter has the potential to reduce of remove the requirement for ground calibration targets; however, this relies on further testing and validation of the absolute temperature measurements made by the modified camera;
- Fly mapping mission with high overlap ($\geq$80%) to account for reduced thermal observations during the flat field correction;
- Post-processing of extra images collected by the sensor should be removed to ensure the first image used in the model is the first image of the flight line, as the largest pixel DN value discrepancy occurs within the first 2–3 min of sensor operation during the 'shock cooling' event;
- We show here that the use of a heated shutter, or some form of insulation around the sensor, should be considered to help alleviate 'shock cooling' events.

5. Conclusions

Drone-acquired thermal imagery using uncooled thermal infrared sensors is subject to substantial temperature errors due to sensor drift. The objective of this study was to assess the efficacy of an uncooled thermal infrared sensor designed for UAS operations and modified with an externally mounted heated shutter. We compared the performance of this modified sensor to an unmodified sensor under both controlled laboratory conditions and an operational field setting over a pine tree plantation.

The modified thermal sensor performed better in terms of temperature accuracy than the thermal sensor alone, in both the field and controlled laboratory trials. The thermal sensor modified with the heated shutter allowed for rapid inflight sensor re-calibration. It was markedly more stable during 'shock cooling' events when airflow was introduced, and showed substantial reduction in observed temperature variability directly after the cooling events. Under laboratory conditions during subsequent airflow events, the modified sensor held within $\pm$5 °C of the blackbody target whereas the unmodified sensor varied $\pm$40 °C from the target temperature. While the absolute temperature performance of the thermal sensors was not directly assessed in the field, we found the variability in temperature data (as measured by standard mean error of thermal image data for each unique coordinate) was substantially smaller using the modified thermal sensor than the thermal sensor alone.

Despite the reduction in thermal observations due to shutter closure, this self-calibrating regime via the heated shutter helped to stabilise temperature drift and compensate for wind conditions common for mapping missions. Using such a system may help to alleviate the need for post-processing based on reference observations acquired in the field. Where precision temperature measurements are required, results from this current investigation suggest that a heated shutter should be integrated with uncooled infrared thermal sensors.

Author Contributions: D.T., A.L., M.M., and J.V. conceived the project. D.T., A.L., and J.V. designed the experimental method and conducted the experiments and data acquisition. J.V., S.Z., G.W., and D.T. analysed the data. J.V. wrote the manuscript draft with contribution from all co-authors. All authors have read and agreed to the published version of the manuscript.

Data Availability Statement: All drone and airborne orthomosaic data, shapefile, and code will be made available on request to the corresponding author's email with appropriate justification.

Conflicts of Interest: The authors declare no conflict of interest.

References

1. Gómez-Candón, D.; Virlet, N.; Sylvain, L.; Jolivot, A.; Regnard, J.L. Field phenotyping of water stress at tree scale by UAV-sensed imagery: New insights for thermal acquisition and calibration. *Precis. Agric.* **2016**, *17*, 786–800. [CrossRef]
2. Hoffmann, H.; Jensen, R.; Thomsen, A.; Nieto, H.; Rasmussen, J.; Friborg, T. Crop water stress maps for an entire growing season from visible and thermal UAV imagery. *Biogeosciences* **2016**, *13*, 6545–6563. [CrossRef]
3. Smigaj, M.; Gaulton, R.; Suarez, J.C.; Barr, S.L. Use of miniature thermal cameras for detection of physiological stress in conifers. *Remote Sens.* **2017**, *9*, 957. [CrossRef]
4. Zarco-Tejada, P.J.; González-Dugo, V.; Berni, J.A. Fluorescence, temperature and narrow-band indices acquired from a UAV platform for water stress detection using a micro-hyperspectral imager and a thermal camera. *Remote Sens. Environ.* **2012**, *117*, 322–337. [CrossRef]
5. Calderón, R.; Navas-Cortés, J.A.; Lucena, C.; Zarco-Tejada, P.J. High-resolution airborne hyperspectral and thermal imagery for early detection of Verticillium wilt of olive using fluorescence, temperature and narrow-band spectral indices. *Remote Sens. Environ.* **2013**, *139*, 231–245. [CrossRef]
6. Baratchi, M.; Meratnia, N.; Havinga, P.J.; Skidmore, A.K.; Toxopeus, B.A. Sensing solutions for collecting spatio-temporal data for wildlife monitoring applications: A review. *Sensors* **2013**, *13*, 6054–6088. [CrossRef]
7. Gonzalez-Dugo, V.; Zarco-Tejada, P.; Nicolás, E.; Nortes, P.A.; Alarcón, J.; Intrigliolo, D.S.; Fereres, E. Using high resolution UAV thermal imagery to assess the variability in the water status of five fruit tree species within a commercial orchard. *Precis. Agric.* **2013**, *14*, 660–678. [CrossRef]
8. Brunton, E.A.; Leon, J.X.; Burnett, S.E. Evaluating the efficacy and optimal deployment of thermal infrared and true-colour imaging when using drones for monitoring kangaroos. *Drones* **2020**, *4*, 20. [CrossRef]
9. Brenner, C.; Zeeman, M.; Bernhardt, M.; Schulz, K. Estimation of evapotranspiration of temperate grassland based on high-resolution thermal and visible range imagery from unmanned aerial systems. *Int. J. Remote Sens.* **2018**, *39*, 5141–5174. [CrossRef] [PubMed]
10. Lhoest, S.; Linchant, J.; Quevauvillers, S.; Vermeulen, C.; Lejeune, P. How many hippos (HOMHIP): Algorithm for automatic counts of animals with infra-red thermal imagery from UAV. *Int. Arch. Photogramm. Remote Sens. Spat. Inf. Sci.* **2015**, *40*, 355–362. [CrossRef]
11. Seymour, A.C.; Dale, J.; Hammill, M.; Halpin, P.N.; Johnston, D.W. Automated detection and enumeration of marine wildlife using unmanned aircraft systems (UAS) and thermal imagery. *Sci. Rep.* **2017**, *7*, 45127. [CrossRef]
12. McCarthy, E.D.; Martin, J.M.; Boer, M.M.; Welbergen, J.A. Drone-based thermal remote sensing provides an effective new tool for monitoring the abundance of roosting fruit bats. *Remote Sens. Ecol. Conserv.* **2021**, *7*, 461–474. [CrossRef]
13. Budzier, H.; Gerlach, G. Calibration of uncooled thermal infrared cameras. *J. Sens. Sens. Syst.* **2015**, *4*, 187–197. [CrossRef]
14. Mesas-Carrascosa, F.-J.; Pérez-Porras, F.; De Larriva, J.E.M.; Mena- Frau, C.; Agüera-Vega, F.; Carvajal-Ramírez, F.; Martínez-Carricondo, P.; García-Ferrer, A. Drift correction of lightweight microbolometer thermal sensors on-board unmanned aerial vehicles. *Remote Sens.* **2018**, *10*, 615. [CrossRef]
15. Flir. Thermal Drone Resources & Training. Available online: https://www.flir.com.au/support-center/training/suas/ (accessed on 3 February 2021).
16. Olbrycht, R.; Więcek, B. New approach to thermal drift correction in microbolometer thermal cameras. *Quant. Infrared Thermogr. J.* **2015**, *12*, 184–195. [CrossRef]
17. Aragon, B.; Johansen, K.; Parkes, S.; Malbeteau, Y.; Al-Mashharawi, S.; Al-Amoudi, T.; Andrade, C.F.; Turner, D.; Lucieer, A.; McCabe, M.F. A calibration procedure for field and UAV-based uncooled thermal infrared instruments. *Sensors* **2020**, *20*, 3316. [CrossRef] [PubMed]
18. Tempelhahn, A.; Budzier, H.; Krause, V.; Gerlach, G. Shutter-less calibration of uncooled infrared cameras. *J. Sens. Sens. Syst.* **2016**, *5*, 9–16. [CrossRef]

19. Flir Tech Note. Available online: https://www.flir.com/globalassets/guidebooks/suas-radiometric-tech-note-en.pdf (accessed on 11 April 2021).
20. Ribeiro-Gomes, K.; Hernández-López, D.; Ortega, J.F.; Ballesteros, R.; Poblete, T.; Moreno, M.A. Uncooled thermal camera calibration and optimization of the photogrammetry process for UAV applications in agriculture. *Sensors* **2017**, *17*, 2173. [CrossRef]
21. Maes, W.H.; Huete, A.R.; Steppe, K. Optimizing the processing of UAV-based thermal imagery. *Remote Sens.* **2017**, *9*, 476. [CrossRef]
22. Torres-Rua, A. Vicarious calibration of sUAS microbolometer temperature imagery for estimation of radiometric land surface temperature. *Sensors* **2017**, *17*, 1499. [CrossRef] [PubMed]
23. Pestana, S.; Chickadel, C.C.; Harpold, A.; Kostadinov, T.S.; Pai, H.; Tyler, S.; Webster, C.; Lundquist, J.D. Bias correction of airborne thermal infrared observations over forests using melting snow. *Water Resour. Res.* **2019**, *55*, 11331–11343. [CrossRef]
24. Olbrycht, R.; Więcek, B.; De Mey, G. Thermal drift compensation method for microbolometer thermal cameras. *Appl. Opt.* **2012**, *51*, 1788–1794. [CrossRef]
25. TeAX. ThermalCapture Calibrator. Available online: https://thermalcapture.com/thermalcapture-calibrator/ (accessed on 10 February 2021).
26. Kelly, J.; Kljun, N.; Olsson, P.-O.; Mihai, L.; Liljeblad, B.; Weslien, P.; Klemedtsson, L.; Eklundh, L. Challenges and best practices for deriving temperature data from an uncalibrated UAV thermal infrared camera. *Remote Sens.* **2019**, *11*, 567. [CrossRef]
27. Acorsi, M.G.; Gimenez, L.M.; Martello, M. Assessing the performance of a low-cost thermal camera in proximal and aerial conditions. *Remote Sens.* **2020**, *12*, 3591. [CrossRef]
28. Ludovisi, R.; Tauro, F.; Salvati, R.; Khoury, S.; Mugnozza, G.S.; Harfouche, A. UAV-based thermal imaging for high-throughput field phenotyping of black poplar response to drought. *Front. Plant Sci.* **2017**, *8*, 1681. [CrossRef] [PubMed]
29. Testi, L.; Goldhamer, D.; Iniesta, F.; Salinas, M. Crop water stress index is a sensitive water stress indicator in pistachio trees. *Irrig. Sci.* **2008**, *26*, 395–405. [CrossRef]
30. Wang, D.; Gartung, J. Infrared canopy temperature of early-ripening peach trees under postharvest deficit irrigation. *Agric. Water Manag.* **2010**, *97*, 1787–1794. [CrossRef]
31. Berni, J.; Zarco-Tejada, P.; Suárez, L.; González-Dugo, V.; Fereres, E. Remote sensing of vegetation from UAV platforms using lightweight multispectral and thermal imaging sensors. *Int. Arch. Photogramm. Remote Sens. Spat. Inform. Sci.* **2009**, *38*, 6.